ANTIREFLECTION COATING FOR SOLAR CELLS BASED ON GRADED-INDEX MATERIALS

Yousef M. A. Adwan[1], Mohammed M. Shabat[1,2], and Guillaume Zoppi[2]

[1] Department of Physics, The Islamic University of Gaza, P.O. Box 108, Gaza Strip, Palestine

[2]Department of Mathematics, Physics and Electrical Engineering, Northumbria University, Newcastle upon Tyne, NE1 8ST, United Kingdom

ABSTRACT. The conversion of sunlight into electricity via photovoltaics presents tremendous opportunities for the generation of renewable energy. However, solar cells still face several challenges and limitations to further reduce manufacturing costs and increase module efficiency. Photon management is paramount to increase the efficiency of the mainstream silicon-based cell and always includes a suitable antireflection coating (ARC) structure to decrease the reflectance (R) at the top surface. We propose a novel triple-layer anti-reflective coating (TLAR) consisting of three layers sandwiched between the upper cover (glass) and the substrate (silicon). The inner three layers are graded refractive index material (GIM)as an active layer, titanium dioxide (TiO_2), and zinc sulfide (ZnS), respectively. The optical properties of the TLAR have been investigated using the transfer matrix method (TMM). The results of using GIM as the active medium, the reflection decays to the minimum value, and the transmittance reaches the maximum values at a specific wavelength range. The proposed triple-layer anti-reflective coating (TLAR) structure presents a promising solution for enhancing the efficiency of solar cells. Its unique design and utilization of graded refractive index material (GIM) as the active layer make it a novel and innovative approach that holds great potential for advancing solar cell technology.

Keywords: solar cell, transfer matrix method, transmission, reflection, and quantum efficiency, ARC.

1. INTRODUCTION

Alternative clean energy sources like photovoltaics have been extensively researched and installed, with current installations reaching 183 GW [1]. However, despite the success of crystalline silicon technologies [1-5], a significant amount of the solar spectrum remains unused. This is due to two main factors: firstly, photons with energy lower than the semiconductor materials (<1.1 eV) are unable to contribute to photocurrent generation, resulting in wasted energy. Secondly, the reflection of sunlight from the solar cell surface is large across the visible spectrum (>30% for silicon), leading to a significant loss of power [2]. To address these issues, modifications to the device structure are needed to maximize photon collection and absorption, thereby reducing surface reflection. This is achieved using anti-reflection coatings (ARC) and modification of the silicon surface. However, impurities in the solar cell from manufacturing processes may still lead to energy losses [2-5].

The primary purpose of ARC is to capture incident light and allow photons to penetrate the semiconductor, maximizing photocurrent and the efficiency of the solar cell by minimizing reflection across the solar spectrum [4-6]. The effectiveness of ARC thin film depends on various criteria such as the chosen material, number of layers, layer thickness, the incident angle of light, and wavelength range over which reflectance needs to be minimized [7-10]. The effective index of refraction of ARC materials falls between the higher and lower indices of constituent materials in bulk state values [8-

9]. While a single layer of SiNx may reduce reflection by more than 20%, multiple layers are generally necessary for optimal performance [5]. It has been observed that small differences in refractive indices between two materials containing a single ARC result in decreased reflection. Double-layer ARC such as SiO2/Si3N4, SiO2/TiO2, ZnO/ZnS, or ZnS/MgF2 have been extensively investigated [6,8-11]. In contrast, the graded refractive index is used to significantly reduce reflectance at dielectric interfaces. The graded layer is divided into sub-layers, each with its volume fraction such that the refractive index is close to the upper and next medium's refractive index. This results in reflectance approaching zero across a wide range of incident angles and wavelengths for the infinite thickness of continuous graded index [12-16]. A double-layer antireflection coating (DLARC) structure was created by depositing Al2O3 on IZO films using an atomic layer deposition system. This DLARC was optimized for SHJ solar cells using wafer ray tracer simulation, resulting in significant improvements over cells with a single-layer IZO film. The DLARC increased current density by 1.37% and efficiency by 0.8% [17]

2. MODEL SOLAR STRUCTURE AND THEORY

Here, we propose a triple-layer anti-reflective coating (TLAR) structure to minimize the reflection across a silicon surface. TLAR consists of three layers sandwiched between a dielectric layer (glass, $n_0 = 1.47$) also referred to as incident media ,and the semiconductor substrate layer (silicon, $n_4 = 3.778 - 0.012i$) as shown in Fig.1 and the inner layers are graded index $n_1 = n_{graded\ index}$, zinc suide (ZnS) ($n_2 = 2.35$) and titanium dioxide (TiO_2) ($n_3 = 2.94$).Three profiles of the graded index can be described by the equation of refractive index [12-16]:

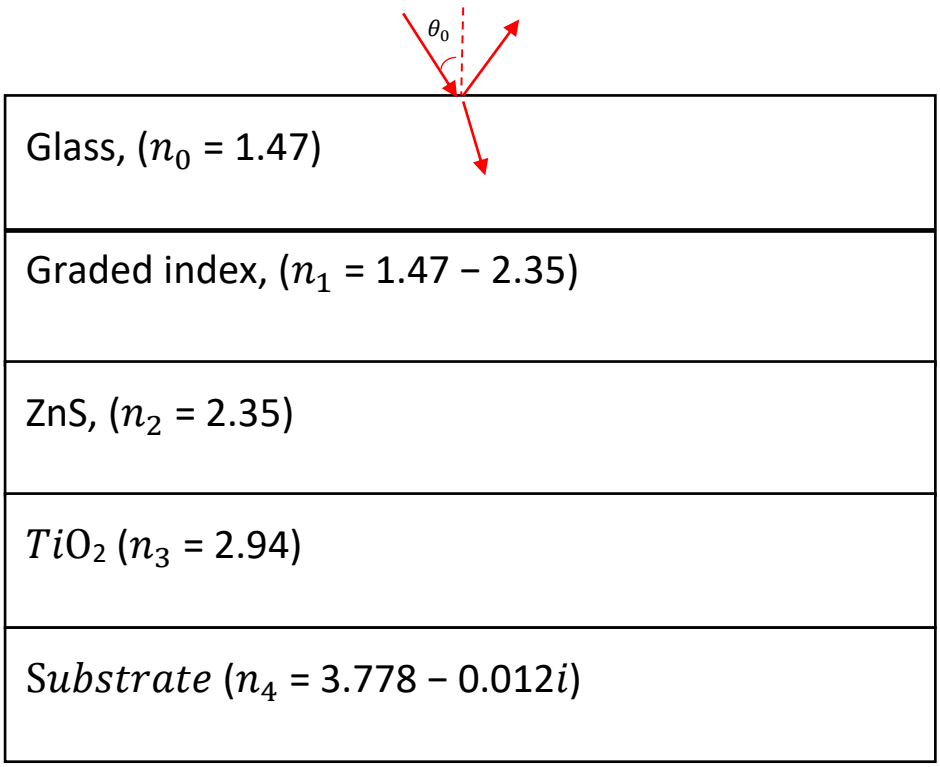

Fig.1 Schematic diagram of the triple-layer anti-reflective coating (TLAR) structure.

Three profiles of the graded index can be described by the equation of refractive index [12-16]:

1 Linear profile:

$$n = n_{low} + (n_{high} - n_{low})x \qquad (1a)$$

2 Cubic profile:

$$n = n_{low} + (n_{high} - n_{low})(3x^2 - 2x^3) \qquad (1b)$$

3 Quintic profile:

$$n = n_{low} + (n_{high} - n_{low})(10x^3 - 15x^4 + 6x^5) \qquad (1c)$$

Where: n_{low}, n_{high} are the refractive indices of an incident medium and the substrate medium, respectively, x is the relative thickness of the ARC in the range, $0 \leq x \leq 1$.

Therefore, the quintic-index profile considers the best approach for the optimal graded-index ARC [12-16]. The transfer matrix method (TMM) is a common and simple method that calculates the field amplitudes interior and exterior to the layers and describes the reflectance and transmittance values across each layer by applying the continuity boundary conditions between the layers [16-20]. Also, it is useful to solve and analyze the interaction of light with the multilayer structure and offers complete control of the physical parameters of ARCs "refractive index and the thickness of each layer" due to the incident and reflected waves from the input layer and the output layer to reach to the lowest possible reflection. Finite difference time domain (FDTD), Fourier model method (FMM), and finite element method (FEM) [18] are other

methods that determine R, T, and absorbance (A) mathematically [18]. The theoretical analysis is used to derive the equations of the R and the T in both, transverse electric mode, (TE), and transverse magnetic field, (TM), by using TMM. This method is one of the easiest and most appropriate methods for this procedure. Following the notations and method of the TMM used previously in [16-20], both T and R spectra have been derived. All the numerical results due to the change in the physical parameters have been solved and plotted using Maple 18.

3. SIMULATION, RESULTS AND DISCUSSION

Fig.2 shows the comparison between the refractive indices for the active layer (n_1) as a function of the relative thickness of the ARC (x) in the linear, cubic, and quantic profiles. We note that the three curves, intersect at x equals (0, 0.5, 1), as the substitution by these values in the three equations will equal the same value of the refractive index.

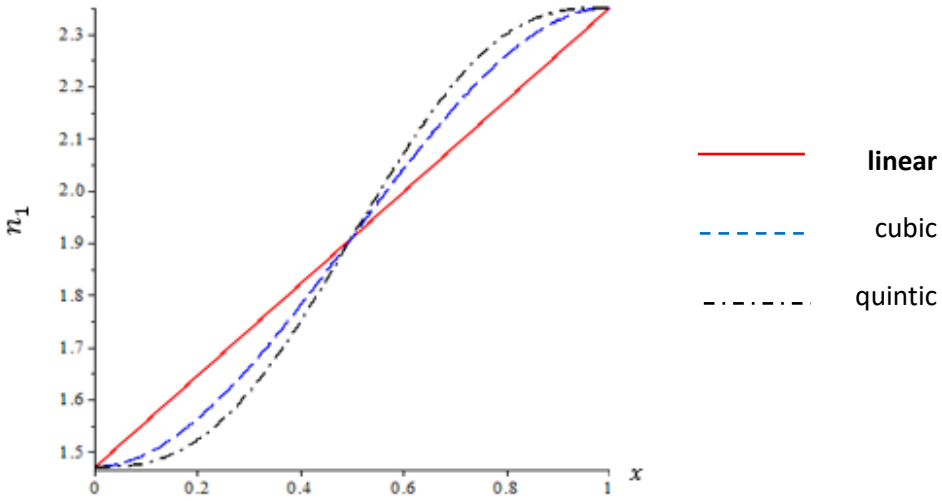

Fig. 2 Refractive indices (n_1) for the linear, cubic, and quantic profiles for different values of x where $0 \leq x \leq 1$ and $n_0 = 1.47$ and $n_2 = 2.35$.

In the case of TE polarization, the reflection and the transmission described have been solved numerically versus the incident wavelength by using three different parameters, namely the relative thickness of ARC in the graded index equation, the incident angle, and ARC thickness.

Fig. 3 illustrates the variation of the reflectance (R) versus the incident wavelength (λ), in normal incidence for different values of the relative thickness of ARC (x) and the different profiles. All figures show that the reflection is large at $x = 0$ and decrease gradually, then increases again gradually to the maximum value at $x = 1$.

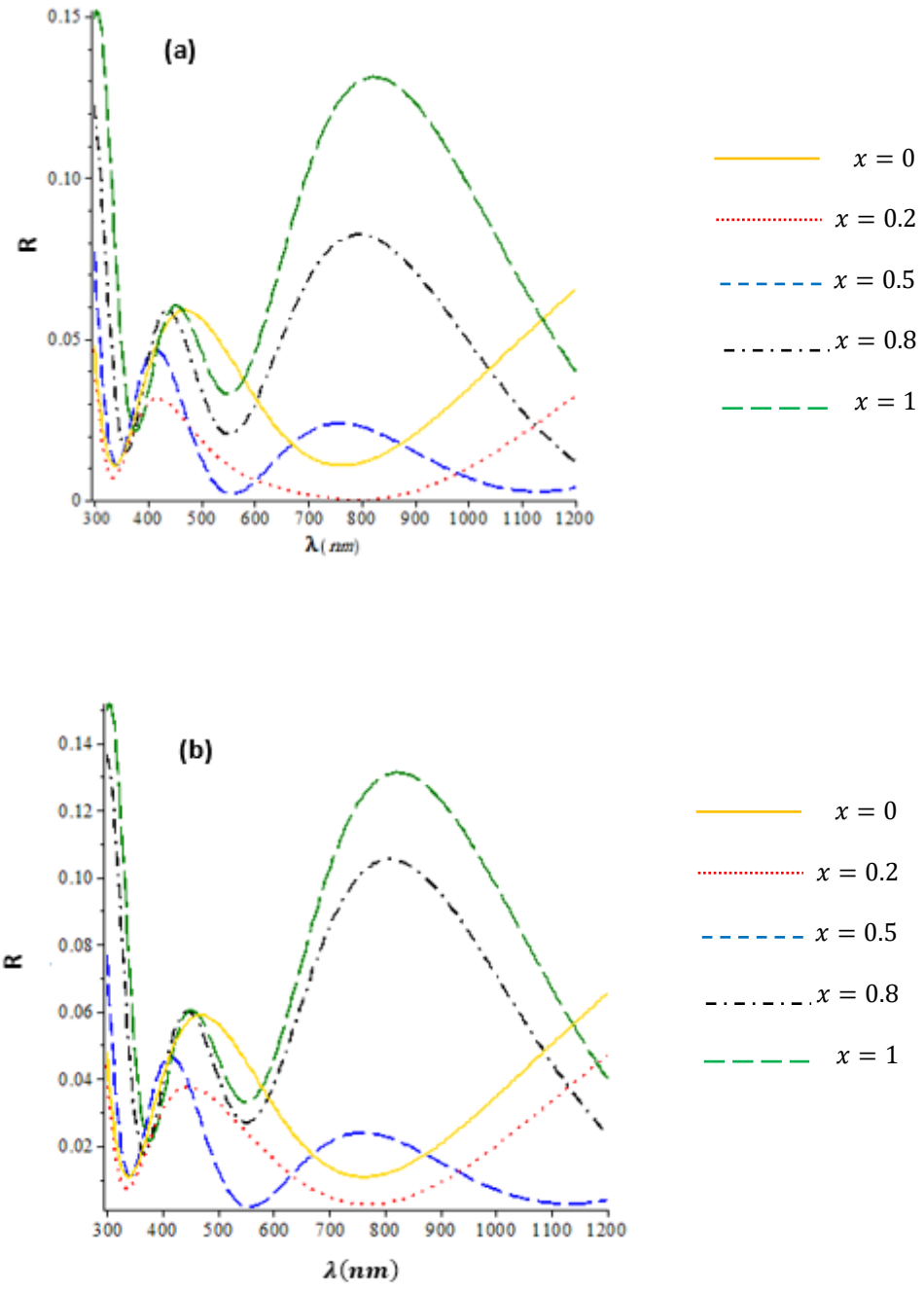

Fig.3: Reflectance (R) of TE polarization versus the incident wavelength (λ) for different values of the relative thickness of ARC (x). (a) For linear profile equation, (b) for cubic profile equation, for $\theta_0 = 0, d_1 = 90\ nm$, $d_2 = 50\ nm$, $d_3 = 40\ nm$.

Fig.4a and 4b display the reflectance versus incident wavelength for the three profiles of the graded index, i.e., linear, cubic, and quintic profiles for the relative thickness of $x = 0.2$ and $x = 0.8$, respectively, in normal incident cases. In both cases, the linear profile expresses the lowest reflection in all spectral ranges of (300-1200 nm) and achieves a remarkable R=0 at a spectral wavelength of 800 nm. On the other hand, the quintic profile expresses the highest reflectance across the spectral range investigated.

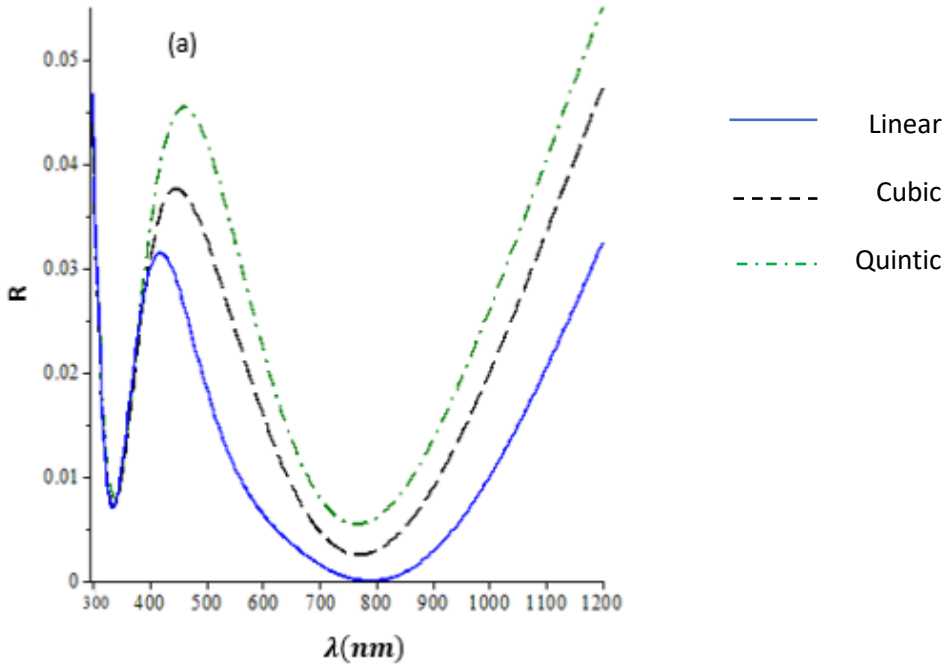

Fig.4a. Reflectance (R) of TE polarization versus the incident wavelength for the three profiles of the graded index linear, cubic, and quintic for $x = 0.2$, $\theta_0 = 0^\circ$,d_1 = 90 nm, d_2 =50 nm, d_3 = 40 nm.

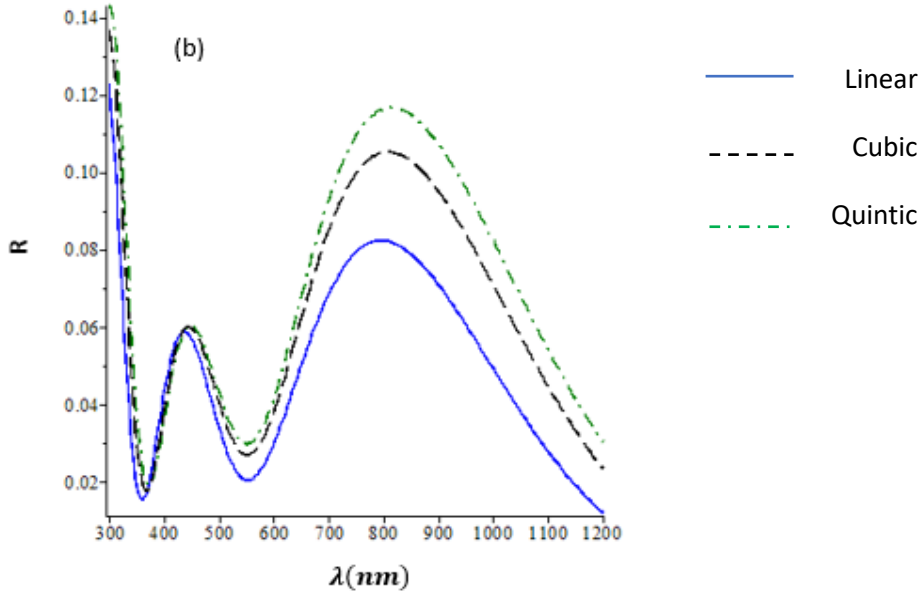

[

Fig.4b Reflectance (R) of TE polarization versus the incident wavelength for the three profiles of the graded index linear, cubic, and quintic for $\boldsymbol{x = 0.8}$, $\boldsymbol{\theta_0 = 0^\circ}$,$d_1$ = 90 nm, d_2 =50 nm, d_3 = 40 nm.

Since the linear profile presents the lowest reflectance, the following study will focus on the linear profile in more depth by investigating the three parameters which are the incident angle (θ), the relative thickness (x), and the layers thickness of the ARC (d). Fig.5 displays the reflectance versus the incident wavelength for different incidence angles (0°,30°, 50°), by using the linear profile equation at $x = 0.3$. The reflectance increases as the incident angles increase over the wavelength range (300-1200 nm). The

maximum reflectance can be obtained in the wavelength range (350-450 nm) which is about 0.035, 0.04, and 0.05 for each value of incidence angles, respectively. The minimum values of reflectance are achieved at $\theta_0 = 0^\circ$ "normal incidence" where the reflectance decreases to 0.005 which is very close to about zero in the wavelength range 550-1000 nm. The minimum spectra have been observed at the wavelength of 850 nm and θ_0 equals 30°.

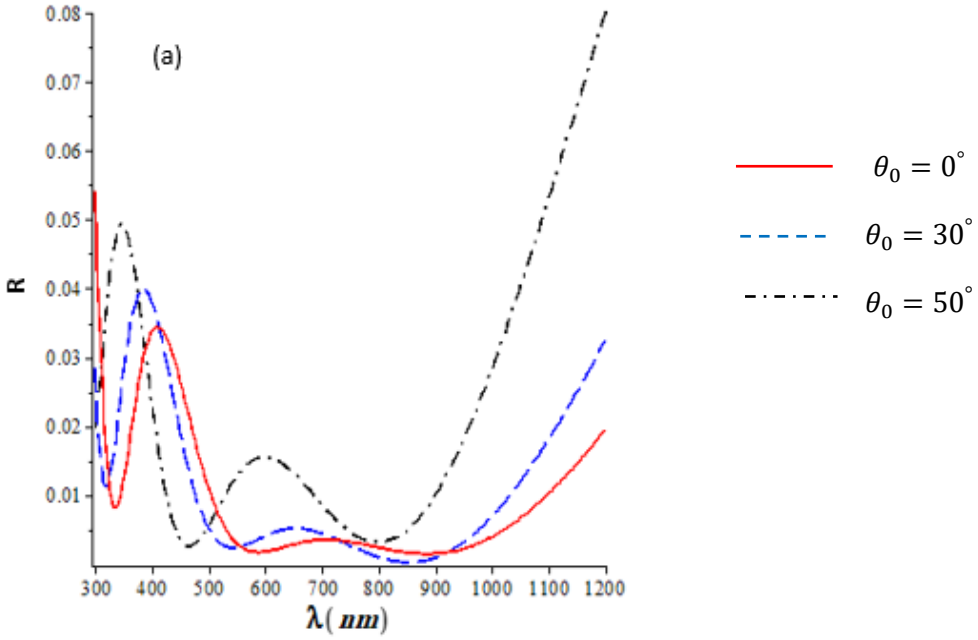

Fig.5a Reflectance (R) of TE polarization versus the incident wavelength for linear profile equation, for different value $\boldsymbol{\theta_0}$ and $\boldsymbol{x} = \mathbf{0.3}$, d_1 = 90 nm, d_2 = 50 nm, d_3 = 40 nm.

Fig.6a illustrates the transmittance (T) versus the wavelength for different incidence angles (0° , 30° , 50°), by using the linear profile equation at $x = 0.3$. At $\boldsymbol{\theta_0} = 0^\circ$, the transmittance reaches a maximum of 1 in the wavelength range of (550-1000 nm).

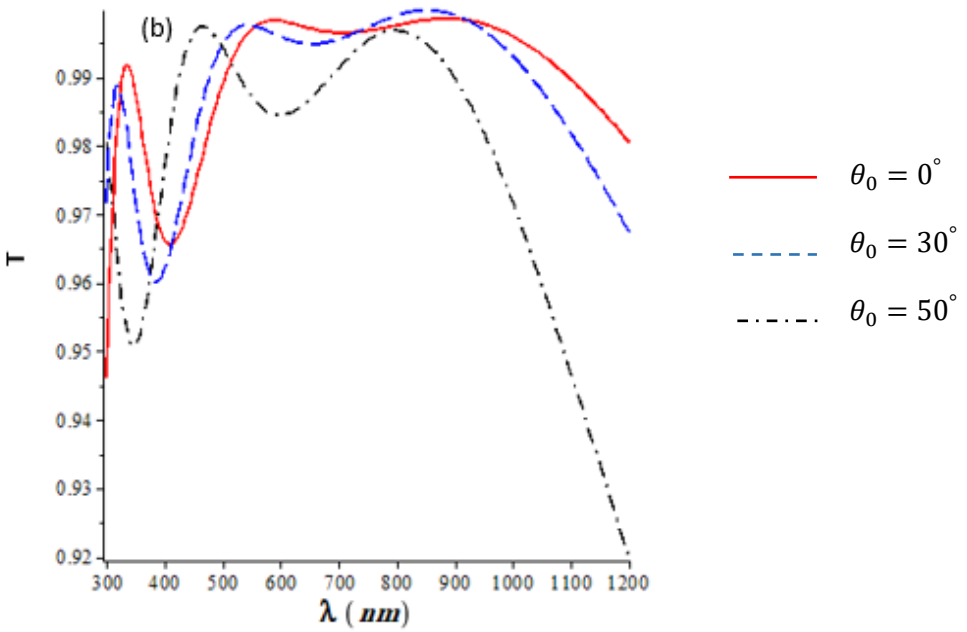

Fig.5b Transmittance (T) of TE polarization versus the incident wavelength for linear profile equation, for different value $\boldsymbol{\theta_0}$ and $\boldsymbol{x = 0.3}$, d_1 = 90 nm, d_2 = 50 nm, d_3 = 40 nm.

Figure 6a shows the reflectance at normal incidence for different thicknesses of the effective medium d1 (40, 90, 150 nm) using the linear profile equation at x=0.3. Reflectance is minimized at d1=90 nm, reaching 0.02 in the wavelength range (550-1000 nm). The highest reflectance values (0.033, 0.034, and 0.057) occur in the wavelength range (400-600 nm) for the investigated thicknesses. Figure 6b displays the transmittance for the same thickness values of d1, reaching maximum values at d1=90 nm and reaching about 1 in the spectral range of 400-600 nm. Both figures demonstrate the importance of the effective medium thickness in determining the optical properties of the material.

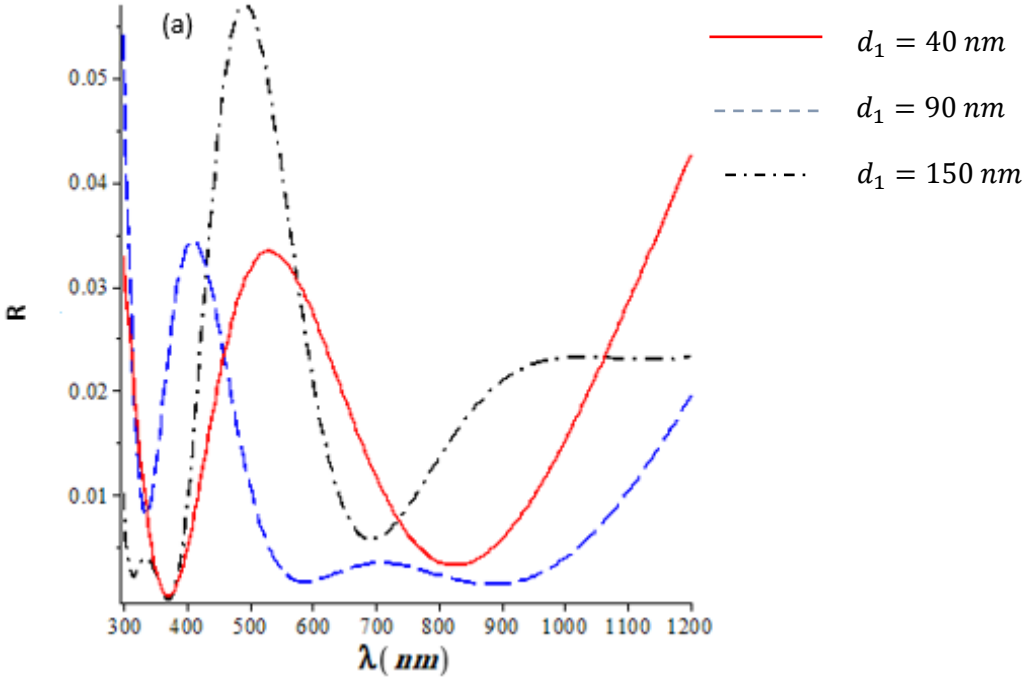

Fig.6a Reflectance (R) of TE polarization versus the incident wavelength for linear profile equation, for a different value d_1, $\boldsymbol{x = 0.3}$, $\boldsymbol{\theta_0 = 0^\circ}$, d_2 =50 nm, d_3 = 40 nm.

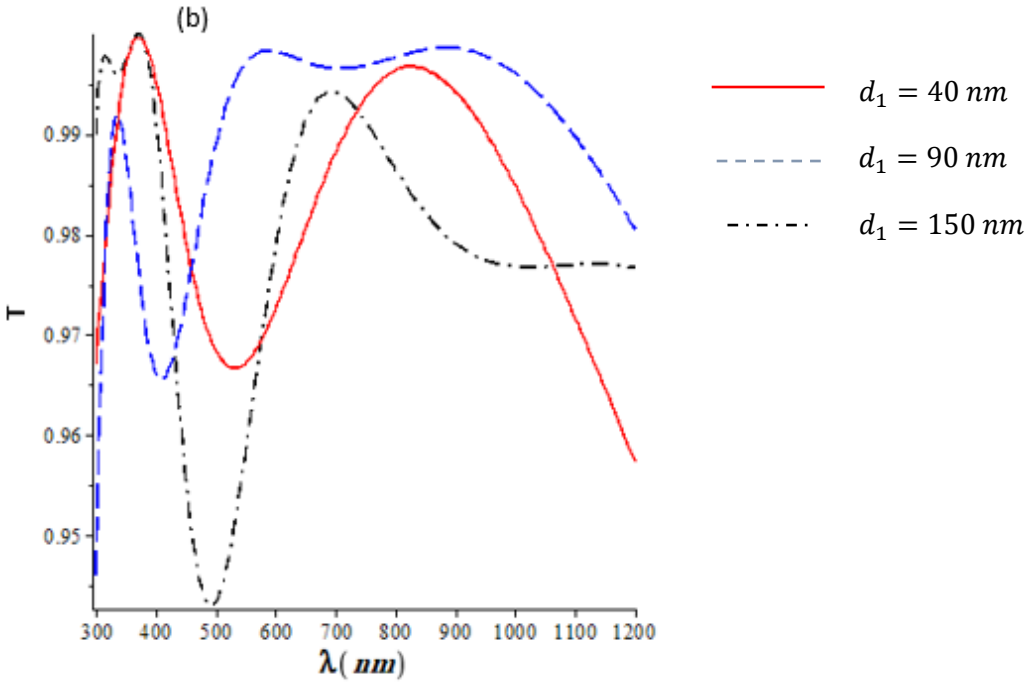

Fig.6b Transmittance (T) of TE polarization versus the incident wavelength for linear profile equation, for a different value d_1, $x = 0.3$, $\theta_0 = 0^\circ$, d_2 =50 nm, d_3 = 40 nm

Similar behavior and characteristics have been achieved for the TM polarization case, so we focus on the TE polarization case.

Fig.7a and 7b show the variation of the reflectance between TE and TM modes at θ 30° , $\theta_0 = 50^{\circ}$ respectively, where the increase in the angle leads to an increase of reflectance in TE polarization and a decrease of the reflectance in the TM polarization c

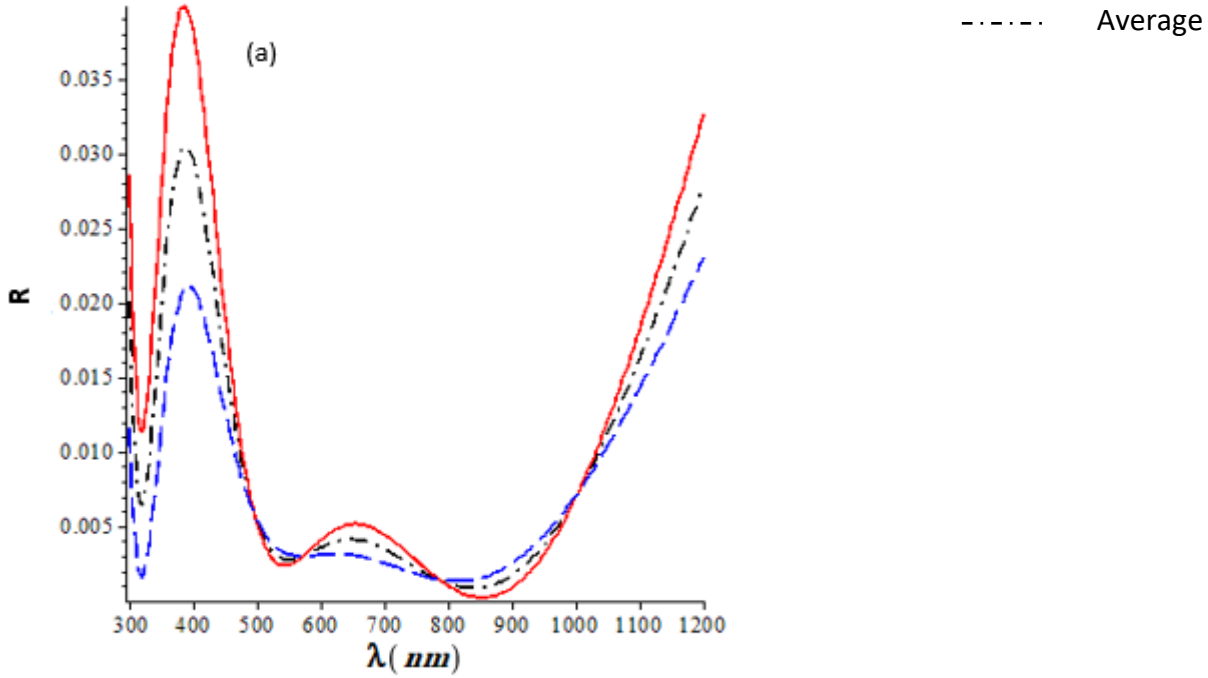

Fig.7a Reflectance (R) of TE, TM polarization, and the average between them versus the incident wavelength for linear profile equation, for $\boldsymbol{\theta_0 = 30^{\circ}}$,$\boldsymbol{x = 0.3}$, d_1 = 90 nm, d_2 = 50 nm, d_3 = 40 nm.

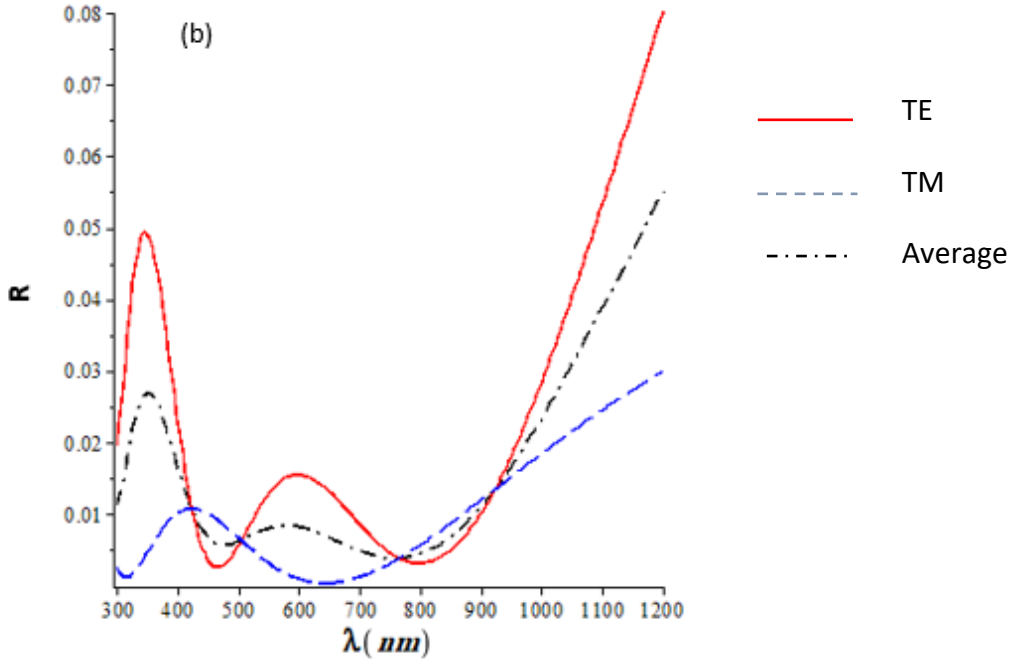

Fig.7b Reflectance (R) of TE, TM polarization, and the average between them versus the incident wavelength for linear profile equation, for $\boldsymbol{\theta_0 = 50^{\circ}}$,$\boldsymbol{x = 0.3}$, d_1 = 90 nm, d_2 = 50 nm, d_3 = 40 nm.

Figures 8a and 8b depict the variation of transmittance with respect to the polarization of the incident light at different incident angles. Specifically, the figures show the transmittance of TE (transverse electric) and TM (transverse magnetic) polarizations at incident angles of 30 and 50 degrees, respectively. As the incident angle increases, the transmittance of the TE polarization decreases, while the transmittance of the TM polarization increases. This effect can be attributed to the way in which the material interacts with the different polarization states of the incident light. In general, materials tend to be more transparent to light with a TM polarization, while they absorb or reflect more of the light with a TE polarization. Therefore, as the incident angle increases, more of the incident light is polarized in the TM direction, resulting in an increase in the overall transmittance for this polarization. Conversely, less light is polarized in the TE direction, resulting in a decrease in the transmittance for this polarization. These effects are reflected in the graphs shown in Figures 8a and 8b.

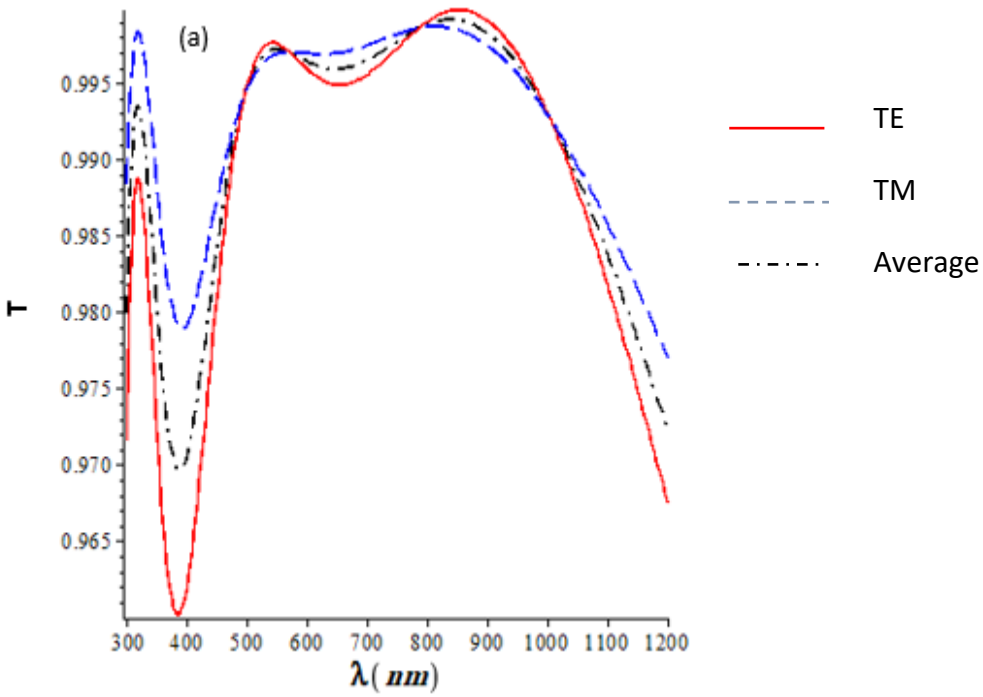

Fig.8a Transmittance (T) of TE, TM polarization, and the average between them versus the incident wavelength for linear profile equation, for. $\boldsymbol{\theta_0 = 30^\circ}$, $\boldsymbol{x = 0.3}$, d_1 = 90 nm, d_2 = 50 nm, d_3 = 40 nm.

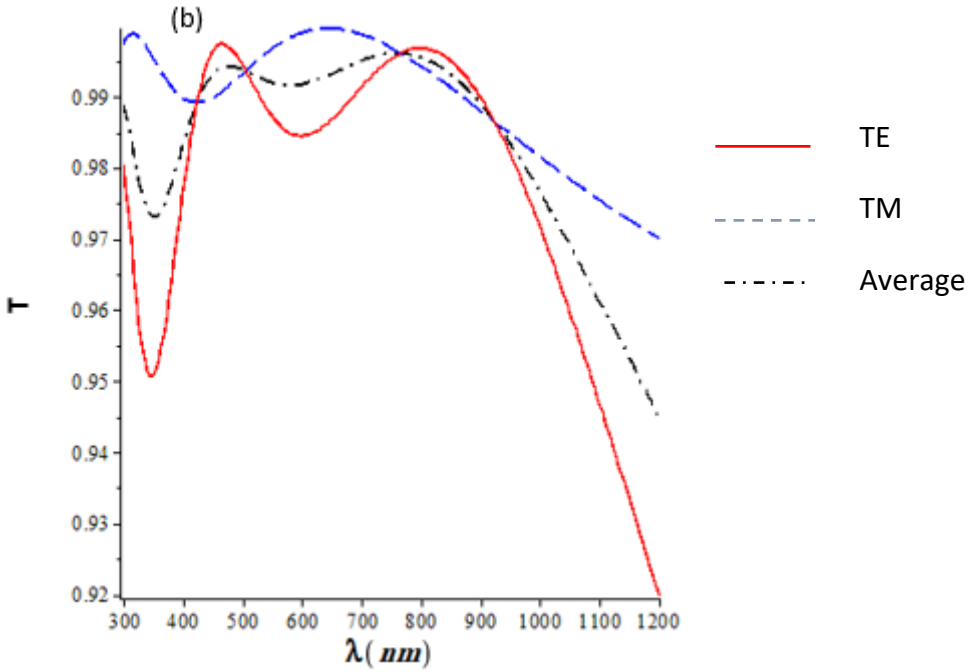

Fig.8b Transmittance (T) of TE, TM polarization and the average between them versus the incident wavelength for linear profile equation, for $\boldsymbol{\theta_0 = 50^{\circ}, x = 0.3}$, d_1 = 90 nm, d_2 = 50 nm, d_3 = 40 nm.

4. SHORT CIRCUIT CURRENT DENSITY J_{sc}

Many factors affect the short circuit current density (J_{sc}) of a solar cell such as the number of photons, the spectrum of the incident light, the surface area of the solar cell, and the collection probability [21,22]. J_{sc} versus the incident angle (θ_0) for different values of thickness, d_1 = 40 nm, 90 nm, and 50 nm, has been solved using the following equation.

$$\mathrm{J_{sc}} = \frac{q}{hc}\int_{\lambda_0}^{\lambda} IQE(\lambda) \times (1 - R(\lambda)) \times \lambda \times AM1.5(\lambda) d\lambda \qquad (2)$$

Where h is Plank's constant, c is the speed of light, q is the elemental charge, $IQE(\lambda)$ is the internal quantum efficiency of the solar cell, λ is the wavelength, $R(\lambda)$ is the measured reflectance, $AM1.5(\lambda)$ is the standard solar spectral irradiance. For an ideal cell where $IQE(\lambda) = 1$. Equation 1 becomes [21,22].

$$\mathrm{J_{sc}} = J_{sc}^{max} \times (1 - R(\lambda)) \qquad (3)$$

Where

$$J_{sc}^{max} = \frac{q}{hc}\int_{\lambda_0}^{\lambda} \lambda \times AM1.5(\lambda) d\lambda \qquad (4)$$

Where $AM1.5(\lambda) = 1000\ Wm^{-2}$ at the standard solar spectral irradiance, for the wavelength range, $300 - 1200\ nm$.Fig.9a displays the maximum J_{sc} values as a function of incidence angle and thickness with maxima at $\theta_0 = 0$ with values of 8.0, 8.7 and 7.95 mA.cm^{-2}. for the three thicknesses investigated. As expected

J_{sc} decreases sharply towards zero at the incident angle reaches 90°.

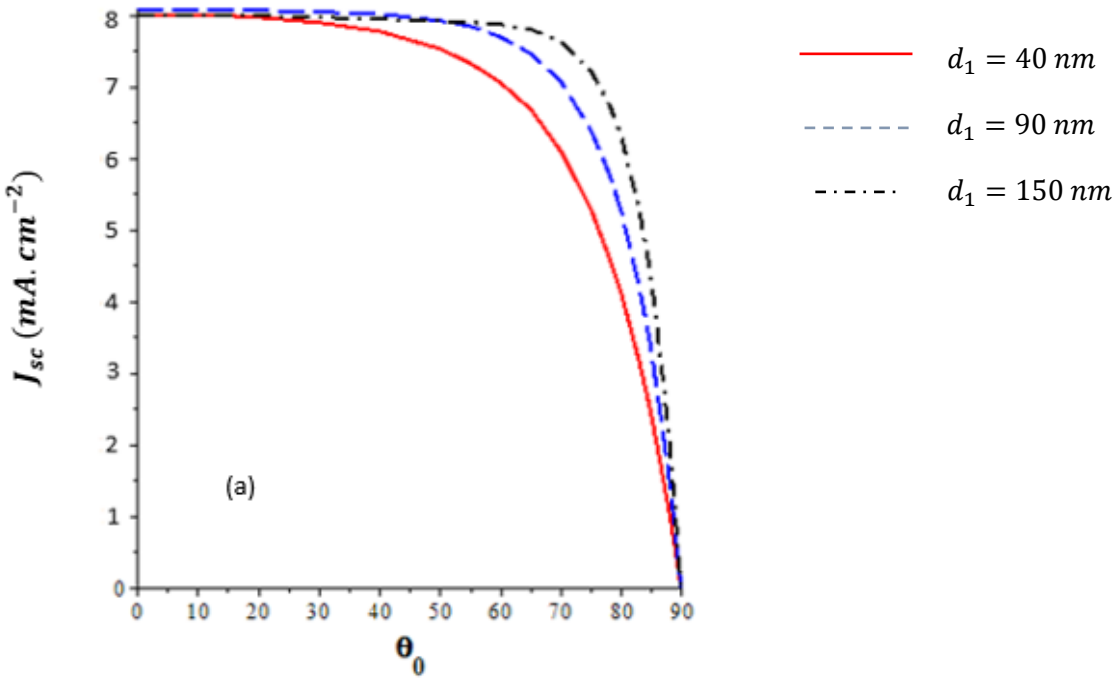

Fig.9a Short current density J_{sc} of TE polarization versus the incident angle θ_0 by using linear profile equation, for different values of thickness, d_1, x = 0.3, d_2 = 50 nm, d_3 = 40 nm.

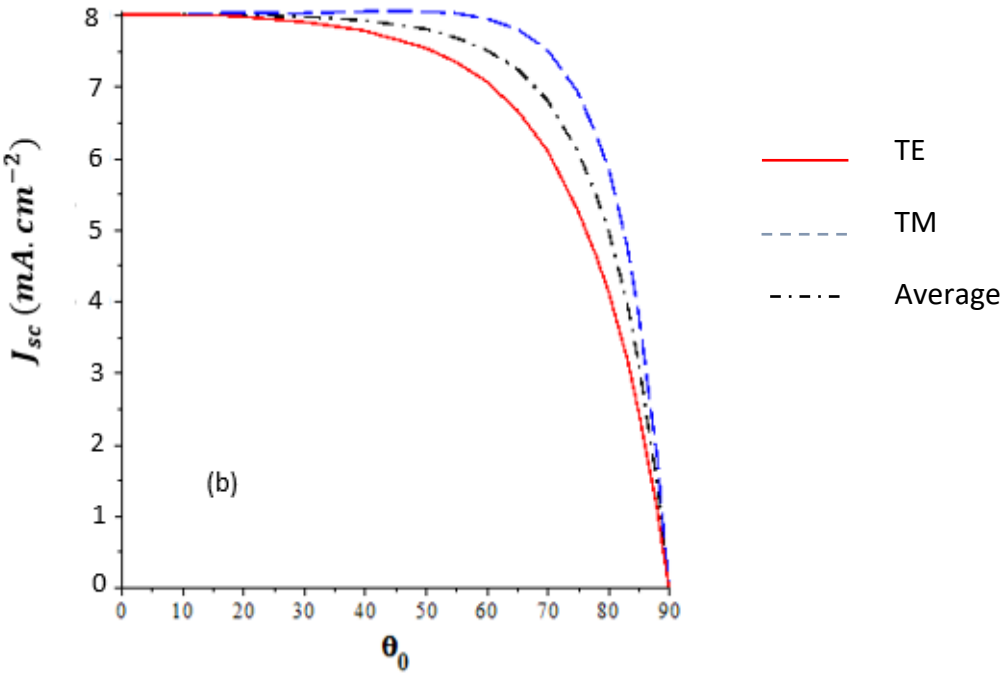

Fig.9b Average of the short circuit current density between TE and TM polarizations versus the incident angle θ_0 by using linear profile equation $x = 0.3$, for different values of thickness d_1 = 40 nm, d_2 = 50 nm., d_3 = 50 nm

The average of the short current density between TE and TM polarizations is plotted versus the incident angle as shown in figure 9b.

5. CONCLUSION

The paper presents the theoretical analysis of the proposed structure of TLARC, which consists of a graded refractive index as an active layer to enhance the performance of the solar cell by decreasing the reflection and increasing the transmittance to the cell. The refractive index for the linear profile equation at $x = 0.3$, for the active layer, is 1.734, which leads to low reflectance reaching. The maximum J_{sc} has been achieved at active layer thickness of $d_1 = 90\ nm$ and incident angle $\theta_0 = 0^{\circ}$. In TE polarization, the incident angle is considered the best angle which satisfies the minimum of the reflection and maximum of the transmittance. So, the increase in the incident angle will decrease the transmittance and increase the reflection. In TM polarization, the incident angle $\theta_0 = 30^{\circ}$ is considered the best case satisfying a minimum reflection and a maximum transmittance for the long range of the wavelength. At $\theta_0 = 0^{\circ}$ in cases of the TE and TM polarization, the reflectance and the transmittance have the same values. Then, the increase in the incident angle will decrease the reflectance in the TM case and will increase in TE polarization. The transmittance in TM polarization is higher than TE polarization under the same conditions except for $\theta_0 = 0^{\circ}$. The proposed structure, which incorporates graded index materials, has demonstrated a high level of transmission and a low level of reflection. This is due to the unique optical properties of these materials, which allow for efficient light transmission through the solar cell. These promising results indicate that the graded index materials have the potential to be used in the design of novel solar cells, with the potential to significantly improve their overall efficiency. By reducing the amount of light that is reflected and increasing the amount that is absorbed by the solar cell, these materials can help to increase the amount of energy that can be harvested from sunlight. As such, the use of graded index materials represents an exciting avenue of research for the development of more efficient and effective solar cells, with important implications for renewable energy generation and sustainability.

Acknowledgment

The authors are grateful to the CARA Fellowship program for financial support.

References

1. Simon Philipps, Photovoltaics *Report*. Fraunhofer Institute for Solar Energy Systems, SE, with the support of PSE Projects GmbH Freiburg, 24 February 2022
2. B. Kumaragurubaran and S. Anandhi, "Reduction of reflection losses in solar cell using Anti Reflective coating," *2014 International Conference on Computation of Power, Energy, Information and Communication (ICCPEIC)*, 2014, pp. 155-157, doi: 10.1109/ICCPEIC.2014.6915357.
3. M. M. Shabat, D. M. El-Amassi, and D. M. Schaadt, *Design and analysis of multilayer waveguides with different substrate media and nanoparticles for solar cells*, Solar Energy Journal 137, 409–412 (2016).

4. C. J. Chen, *Physics of Solar Energy*, John Wiley & Sons, Inc., Hoboken, New Jersey, 2011
5. M.F. Beye, A. Faye, F. Ndiaye, Ndiaye and A. Seidou Maiga , *Optimization of SiN_x Single and Double Layer ARC for Silicon Thin Film Solar Cells on Glass*, Research Journal of Applied Sciences, Engineering and Technology **6(3):** 412-416, 2013
6. Al Montazer Mandong Abdullah Uzum, *Fresnel calculations of double/multi-layer antireflection coatings on silicon substrates*, Res. Eng. Struct. Mat. Vol. 7 Iss. 4 539-550 539 (2021)
7. H. M. Mousa, M. M. Shabat, and M. R. Karmoot, *Double layer antireflection coating design for conductive solar cells*, Romanian Reports in Physics **72**, 416 (2020).
8. D. Bouhafs, A. Moussi, A. Chikouche, J. M. Ruiz, *Design and Simulation of Antireflection Coating Systems for Optoelectronic Devices: Application to Silicon Solar Cells*, Solar Energy Materials & Solar Cells, **52**: pp. 79-93 (1998)
9. Mamadou Moustapha Diop, Alassane Diaw, Nacire Mbengue, Ousmane Ba, Moulaye Diagne, Oumar A. Niasse, Bassirou Ba, Joseph Sarr, Optimization and Modeling of Antireflective Layers for Silicon Solar Cells: In Search of Optimal Materials, Materials Sciences and Applications, Vol.9 No.8, July 2018
10. Sahouane Nordine, Abdellatif Zerga, *Optimization of Antireflection Multilayer for Industrial Crystalline Silicon Solar Cells*, Energy Procedia 44:118–125, (2014)
11. K. Q. Salih and M.R. Hashim, *Modelling and simulation study of visible emission transmissivity of silicon related to single and multilayer antireflection coatings*, J. Physical Science, **17(2),** 15–26, (2006)
12. Y. Zhao, F Chen, Q. Shen, L. Zhang, *Optimal Design of Graded Refractive Index Profile for Broadband Omnidirectional Antireflection Coatings Using Genetic Programming*, Progress in Electromagnetics Research, **145(10):** pp. 39-48 (2014)
13. Al Montazer Mandong1, Abdullah Uzum, *Fresnel calculations of double/multi-layer antireflection coatings on silicon substrates*, Res. Eng. Struct. Mat. Vol. 7 Iss. 4, 539-550 (2021)
14. GuoJiao Hou, Iván García, Ignacio Rey-Stolle, High-low refractive index stacks for broadband antireflection coatings for multijunction solar cells, Solar Energy, Volume 217, Pages 29-39, (2021)
15. M. Lipinski, A. Kaminski, J.-François Lelièvre, P. Zieba, *Investigation of graded-index SiOxNy antireflection coating for silicon solar cell manufacturing*, Physica Status Solidi (C) Current Topics in Solid State Physics **4(4):**1566 – 1569, (2007)
16. M. M. Shabat and Y. Adwan, *Optical simulations of Graded Index Materials for solar cells model structure*, *TE*, 2020 *International Conference on Promising Electronic Technologies (ICPET)*, Jerusalem, Palestine, 2020, 99-102, (2020)
17. Zhang Jun-Chao, Xiong Li-Min , Fang Ming and He Hong-Bo, Wide-angle and broadband graded-refractive-index antireflection coatings, Chinese Physics B, **22(4)**: 044201 (2013) 04420
18. M. F. Ubeid, M. M. Shabat, *High efficiency solar cells of multi-layered organic structures*. Journal of Nanoelectronics and Optoelectronics, **13**: 1175–1180 (2018)
19. H. Hamouche and M. M. Shabat, *Enhanced absorption in Silicon-Metamaterials waveguide structure*, Applied Physics A **122**, 685 (2016)

20. M. F. Ubeid, M. M. Shabat, and J. Charrier, *Antireflection coatings comprised of metal nanoparticles and silicon nitride*, Romanian Reports in Physics **72**, 415 (2020).
21. M. M. Shabat, S. A. Nassar, and H. G. Roskos *Modeling plasmonic solar cells with noble metal nanoparticles using the finite difference time domain method*, Romanian Journal of Physics **65**, 609 (2020).
22. M. F. Ubeid and M. M. Shabat, *Reflection and transmission of electromagnetic waves by a multilayered solar cell containing organic materials*, Optical and Quantum Electronics **51**, 197 (2019)
23. Mohammed M. Shabat, Sahar M. Abu Ibaid, and Hana M. Mousa**,** *The effects of triple-layer Anti-reflection coating on current density of solar cell*, Romanian Journal of Physics**, 66**, 606 (2021)
24. F. Cortes-Juan, C. Chaverri Ramos, J.P. Connoll, C. David, *Effect of Ag nanoparticles integrated within antireflection coatings for solar cells*, Journal of Renewable and Sustainable Energy, **5**, 033116 (2013)